Hindawi
Geofluids
Volume 2021, Article ID 5542447, 16 pages
https://doi.org/10.1155/2021/5542447

Research Article

Jurassic Terrestrial Shale Gas Potential of the Northern Kashi Sag in the Tarim Basin, Northwestern China

Wei Wu,[1] Zhiwei Liao,[2] Honghan Chen,[1] Shaohu Li,[1] Ao Su,[3] Irshad Hussain,[1] and Niubin Zhao[1]

[1]*Department of Petroleum Geology, School of Earth Resources, China University of Geosciences (Wuhan), Wuhan 430074, China*
[2]*State Key Laboratory of Coal Mine Disaster Dynamics and Control, School of Resources and Safety Engineering, Chongqing University, Chongqing 400044, China*
[3]*Department of Petroleum, School of Geosciences, Yangtze University, Wuhan 430100, China*

Correspondence should be addressed to Zhiwei Liao; zwliao16@cqu.edu.cn

Received 29 January 2021; Revised 1 April 2021; Accepted 7 June 2021; Published 3 August 2021

Academic Editor: Kun Zhang

Evaluation of terrestrial shale gas resource potential is a hot issue in unconventional oil and gas exploration. Organic-rich shales are widely developed in the Jurassic strata of Tarim Basin, but their shale gas potential has not been described well. In the study, the Lower-Middle Jurassic fine-grained sedimentary rocks (Kangsu and Yangye Formations) in northern Kashi Sag, northwestern Tarim Basin, were taken as the study object. The comprehensive studies include petrology, mineralogy, organic geochemistry, and physical properties, which were used to characterize the organic matter and reservoir characteristics. Results show that the Jurassic terrestrial shale in the northern Kashi Sag was mainly deposited in lakes, rivers, and deltas. The thickness of black lacustrine shale developed in the Early-Middle Jurassic in the study area is generally over 100 m. The total organic carbon (TOC) content is rich, averaging 2.77%. The vitrinite reflectance (R_o) values indicate that the Lower Jurassic shale organic matter is in the early mature–mature stage, while the Middle Jurassic is in the mature stage. Besides, organic matter is primarily II and III in kerogen types. The whole shale contains a large number of clay minerals, especially illite. The average brittle minerals such as quartz and feldspar are 28.67%, and the average brittleness index is 38.63%. Nanoscale pores containing intergranular pores, dissolution pores, and organic pores, coupled with microcracks, are well developed in Jurassic shale. The sample's average pore volume is 0.017 cm^3/g, and the specific surface area is 9.36 m^2/g. Mesoporous contribute the most to pore volume, while the number of microporous is the largest. Both of them provide most of the surface area for the shale. Combined with regional geologic settings, we propose that the Jurassic terrestrial shale has good-excellent shale gas exploration potential and development prospects.

1. Introduction

The remarkable success of shale gas in North America led to the vigorous development of shale gas exploration and increased the investigation of global shale gas potential, thus changing the world energy pattern [1–5]. In recent years, China has also made rapid development in shale gas, and commercial shale gas fields such as Fuling, Changning-Weiyuan, and Zhaotong have been discovered in South China [6, 7]. With the deepening of exploration and development, the pressure to increase shale gas reserves and production in the future is still tremendous. There is an urgent need to expand new fields and strata. The continental basins in China are widely distributed, and the continental shale is developed in many strata such as Mesozoic-Cenozoic [8–11], which is one of the required replacement fields for shale gas exploration. Industrial discoveries of continental shale gas are found in several Triassic stratigraphic wells in Ordos Basin and Jurassic strata in Sichuan Basin [12, 13]. However, compared with marine shale, the output of continental shale gas is lower. Due to the limitation of low exploration degree and complex reservoir conditions [8, 14–16], the large-scale exploration and development of continental shale gas still need further research.

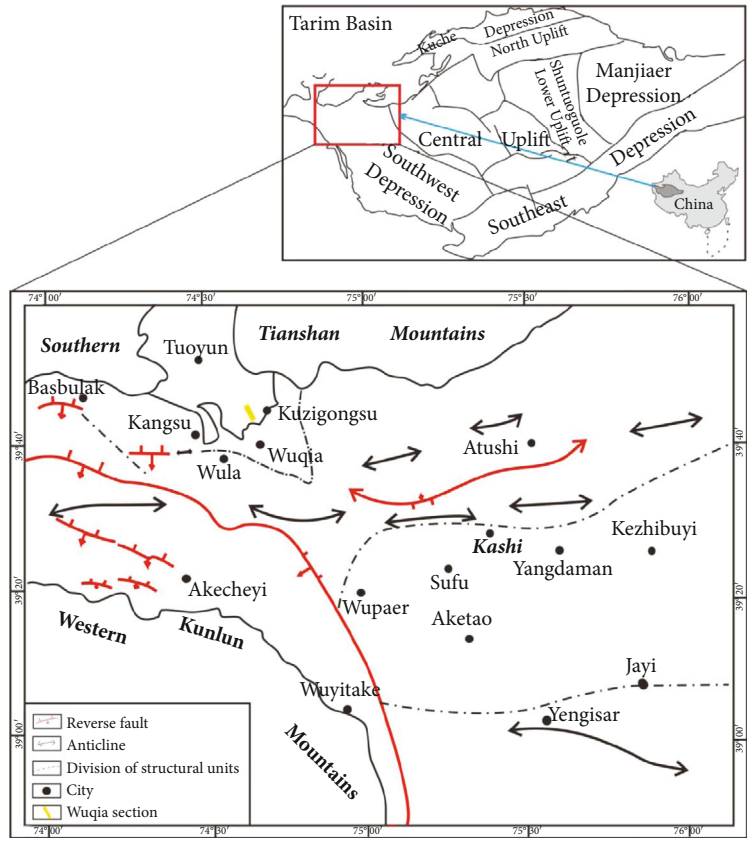

Figure 1: Location of the study area and the structure outline map of the Kashi Sag in Tarim Basin, northwestern China (after [34]).

There is a good prospect for oil and gas exploration in Kashi Sag of Tarim Basin [17–19]. Thick Jurassic organic-rich continental shale was deposited in this area, but no major hydrocarbon exploration breakthrough has been made so far. Previous studies show that source rocks are developed in Kashi Sag from Paleozoic to Cenozoic [20–22], such as Cambrian-Ordovician, Carboniferous-Permian, Jurassic, and Upper Cretaceous-Paleogene. Among them, Jurassic source rocks and Carboniferous-Permian source rocks are considered the two primary source rocks in the study area [23–25]. Concretely, the former is mainly composed of continental fine-grained sedimentary rocks, with a wide area, large thickness, high organic matter content, and good hydrocarbon generation potential [26, 27]. It is considered the most favourable shale gas development area in Tarim Basin [28, 29].

However, there are few detailed studies on Jurassic continental shale gas in this area, and it is urgent to carry out more related researches. On this basis, this study takes the Middle and Lower Jurassic Kangsu Formation and Yangye Formation in Kashi Sag, Tarim Basin, as research objects and comprehensively uses petrology, mineralogy, and organic geochemistry to analyze the organic matter and reservoir characteristics of continental shale, which provides a reference for exploration and preliminary evaluation of shale gas resources in Kashi Sag.

2. Geological Background

Kashi Sag is located in the north of Southwest Depression in Tarim Basin. Since Sinian (Ediacaran), its paleogeography and structural pattern have been controlled by Tarim Plate, South Tianshan Mountains, and West Kunlun Mountains [30, 31]. This sedimentary depression is adjacent to the piedfort thrust belt of West Kunlun Mountains in the west and the Maigaiti slope in the east. Tianshan Mountains and West Kunlun Mountains converge in the west of the study area, which covers about 2.44×10^4 k m^2 [32, 33]. In the south and north Kashi Sag, there are fold-thrust belts in the northern margin of West Kunlun Mountains and the southern margin of South Tianshan Mountains, respectively, which overlap and influence each other in the west of Wuqia County (Figure 1). The northern fold-thrust belt is characterized by east-west segmentation and north-south discontinuity, while the southern fold-thrust belt shows a typical strike thrust nappe structure. According to the study of Zhou et al. [34], Kashi Sag can be divided into four structural units: Kashi deep Sag, South Tianshan piedmont fold-thrust belt, Kuzigongsu Late Triassic-Middle Jurassic fault depression, and West Kunlun piedmont fold-thrust belt.

Kashi Sag, together with the whole Tarim Basin, is a relatively stable platform during the Paleozoic period, consisting of shallow sea carbonate rocks and terrigenous clastic rocks [31, 35]. In the Early Permian, the Eurasian, South

Tianshan, and West Kunlun orogenic belts were gradually formed under the influence of the late Hercynian tectonic movement, resulting in the absence of Late Permian and Triassic strata in Kashi. After the Early Jurassic, the southwestern Tarim Basin has entered the continental sedimentary period [36–38]. The Lower Jurassic Shalitashi Formation (J_{1s}) and Kangsu Formation (J_{1k}) are mainly variegated conglomerates and coal seam, containing plant fossils, indicating the sedimentary environment of near-source alluvial fan, braided river delta, and shallow lake. The Middle Jurassic Yangye Formation (J_{2y}) and Taerga Formation (J_{2t}) are mainly composed of gray mudstone intercalated with a conglomerate in lithology, which belongs to fan delta, braided river, and shore-shallow lacustrine deposits [39–41]. Generally speaking, the Early and Middle Jurassic is mainly continental coal-bearing clastic rock deposits and coastal shallow lake deposits. All kinds of sediments are distributed in strips along the front of the Kunlun Mountains, which is related to the types of sedimentary basins. Kashi Sag's sediments are distributed in a ring shape, with shallow lake facies at the center and rivers and alluvial fan facies at the periphery [42]. During the Late Jurassic, Tarim Craton Basin's sedimentary pattern did not change significantly; i.e., the Upper Jurassic Kuzigongsu Formation (J_{3ku}) is mainly conglomerate interbedded with mudstone conglomerate and sandstone in lithology, indicating an alluvial fan environment. Based on previous studies, the main development horizons of Jurassic terrigenous shale in Kashi Sag are the Lower Jurassic Kangsu Formation and Middle Jurassic Yangye Formation (Figure 2).

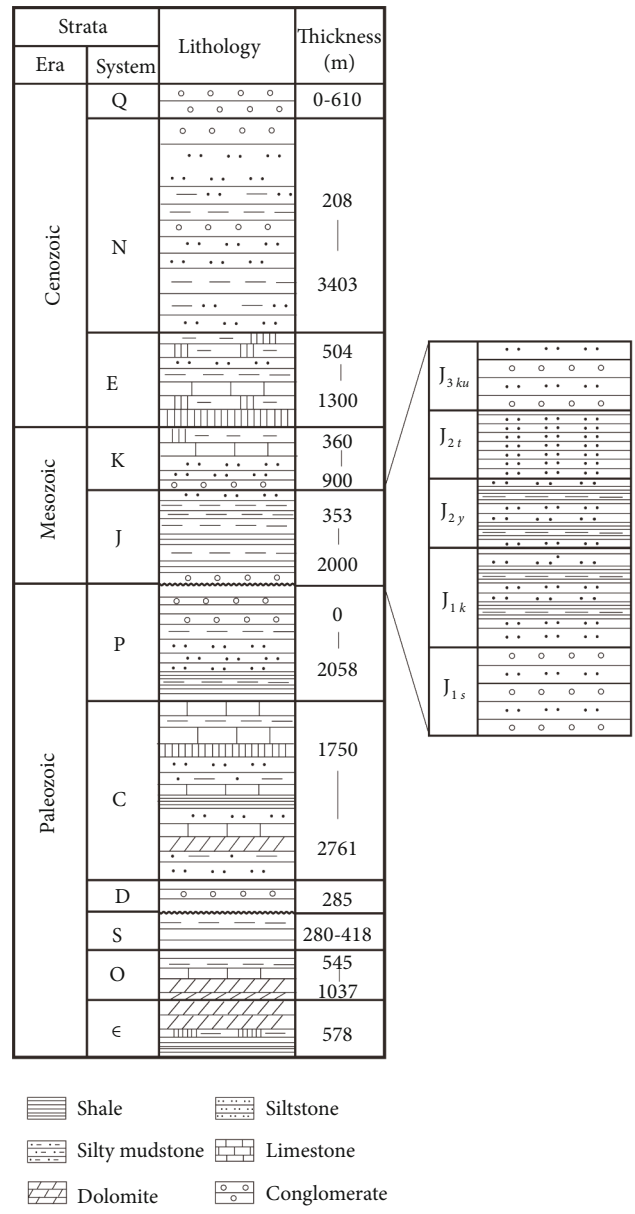

Figure 2: Comprehensive stratigraphic column of Kashi Sag in Tarim Basin (after [34]).

3. Samples and Methods

Six outcrop samples were collected in the north of Wuqia County, Kizilsu Kirgiz Autonomous Prefecture, Xinjiang, China. These samples are numbered from WQ-01 to WQ-06, of which four (WQ-01–WQ-04) are from the Kangsu Formation, and two are from the Yangye Formation (WQ-05–WQ-06) (Figure 3). Analyses of total organic carbon (TOC), vitrinite reflectance (R_o), mineral composition, and absorption-desorption capability were conducted to characterize their organic matter features and reservoir properties. To minimize the potential effects of surface weathering and contamination, all of the collected samples used for analyses were freshly cut after removing the weathered surface.

TOC and X-ray diffraction (XRD) analyses of the samples were carried out at the Xinjiang Mineral Experiment Research Institute (XMERI), China. First, each specimen was split and pulverized into more delicate powders in an agate mortar than the size of the 200 mesh. We weighed approximately 200 mg of powder and processed it at 60°C to dissolve carbonate with 10 percent hydrochloric acid (HCl). We cleaned the samples with deionized water after that and dried them for 12 hours. Finally, the samples were analyzed by a carbon-sulfur analyzer XKSY-SB-646 to determine total organic carbon content. The analytical error was reported to be better than 1% based on replicate analyses of the Chinese national standard GB/T 19144-2010. A D/max-2600 X-ray diffractometer was used to test the mineral composition of samples in the study. In the copper holders, powdered samples were placed and screened for full-rock design from 5 to 90° and clay-fractional composition from 3 to 30°. We used Cu K-α radiation and a 2° min^{-1} graphite monochromator with 0.02° stage diameter and higher analytical accuracy than 0.02°.

The R_o, scanning electron microscopy (SEM), energy-dispersive spectroscopy (EDS), and isothermal adsorption experiments were conducted in the Key Laboratory of Tectonics and Petroleum Resources of the Ministry of Education, China. For R_o measurements, the polished sections were measured using Leica DM4500P polarimetric microscope and CRAIC 308 PV microphotometer.

Six thin sections were highly polished using a Gatan Model 697, Ilion II Broad Beam Argon Milling System. The

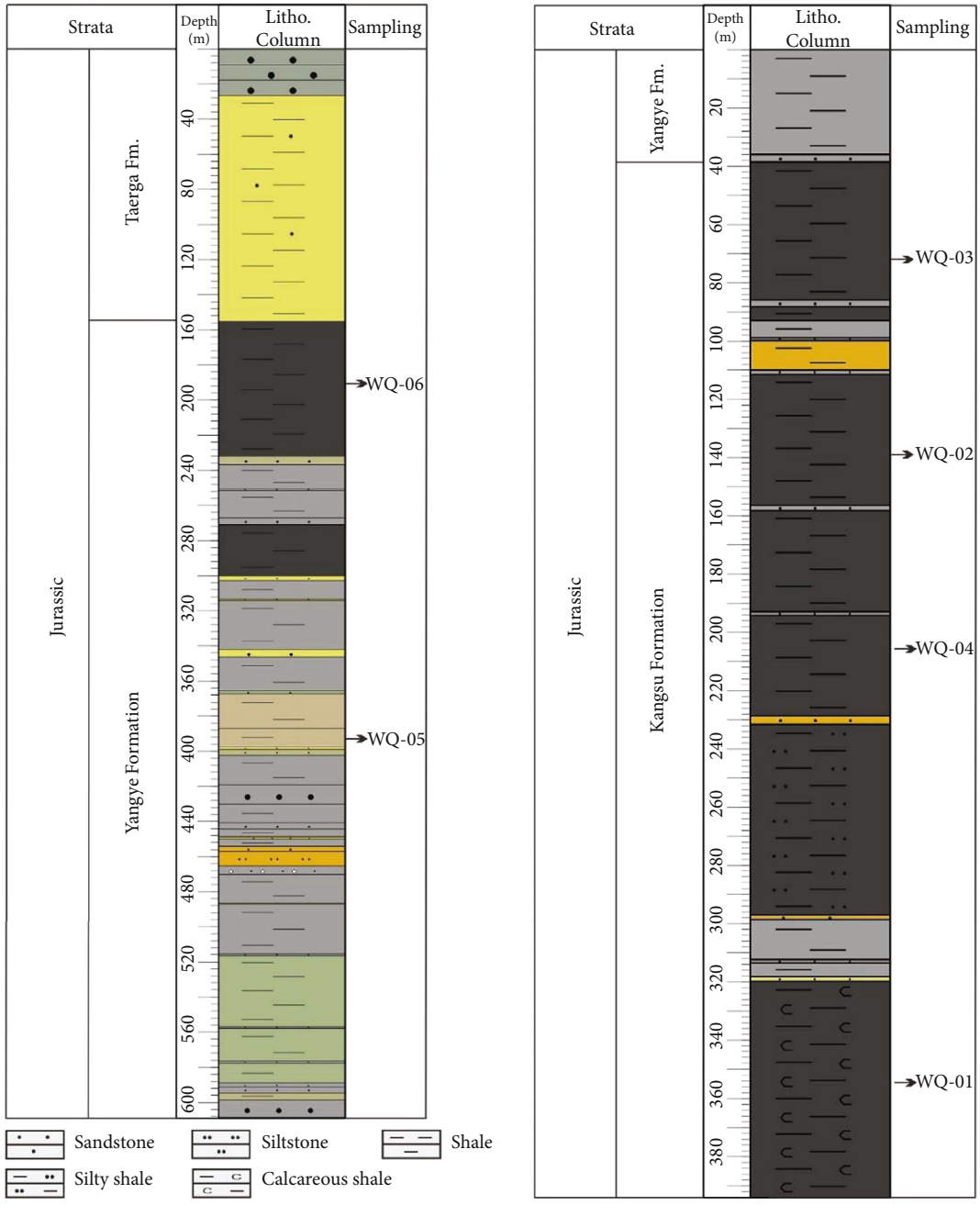

Figure 3: Stratigraphic column of Wuqia County north section in Tarim Basin.

EVO LS 15 scanning electron microscope and AZTEC X-MAX 20 spectrometer were used to identify and analyze the morphological characteristics of minerals and pores. Isothermal adsorption experiments of liquid nitrogen were carried out in this study. 5-10 g of screened powder samples with particle size between 0.28 and 0.45 mm was selected and then baked at 105°C for 8 hours. Finally, the samples were measured by a fully automatic surface and porosity analyzer ASAP2020.

4. Results

In this study, the detailed outcrop section in the Wuqia area was investigated in the field. The northern section of Wuqia County is located about 6 km northwest of Wuqia County, near Kangsu Coal Mine (Figure 1). The measured section length is approximately 1.3 km, and the actual thickness of the stratum is about 1000 m. The exposed strata are mainly the Jurassic Kangsu Formation and Yangye Formation in ascending order. Due to terrains, this section is divided into two sections for field observation (Figure 3).

4.1. Petrologic Feature. The lithology of the Kangsu Formation is dominated by black-gray mudstone, black carbonaceous mudstone, and dark siltstone, interbedded with conglomerate rock (Figures 4(a) and 4(b)). The thickness of shale is the highest lithology in the Kangsu Formation, with

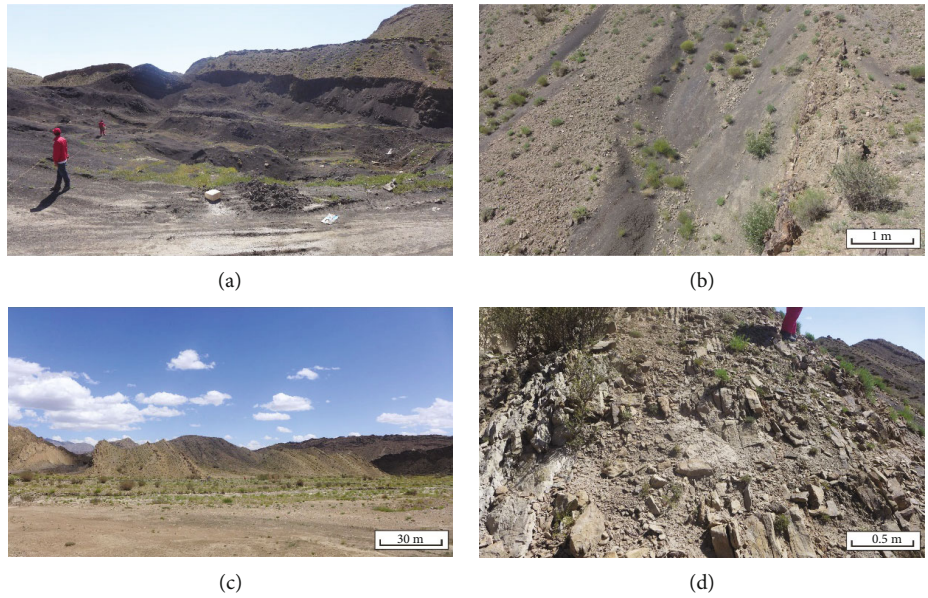

(a) (b) (c) (d)

Figure 4: Lithological characteristics of the Kangsu Formation and Yangye Formation of Wuqia section. (a) Full view of the Kangsu Formation. (b) Black carbonaceous mudstone in the Kangsu Formation. (c) Complete view of the Yangye Formation. (d) Gray siltstone in the Yangye Formation.

a total of 245 m. The rocks are mainly gray and dark in colors, and mudstone often contains lenticular siderite, reflecting the weak oxidation-weak reduction environment. Gravels are poorly sorted, and particle sizes are generally distributed in 2–6 cm, and some larger ones can reach 10 cm. Their roundness is good, which is generally subround–round. From the point of view of sedimentary sequence, the grain size of whole section gradually becomes finer upward, which is reflected as a transgressive process. This situation may be related to the extensional tectonics in Kashi Sag during the Early Jurassic period [40, 41]. When the crust continuously extended and thinned horizontally, which caused regional subsidence, this results the lake basin expansion and water level rise. The above petrological traits display that the sedimentary environment of the study area in this period is mainly rivers, shallow lakes, and deltas around the lake basin.

The boundaries of the Yangye Formation and Kangsu Formation are conformable contacts, and the Yangye Formation is often unconformably contacted with Paleozoic strata in general. In the Wuqia section, the Yangye Formation is primarily composed of dark gray mudstone and black carbonaceous mudstone, interbedded with greyish-green medium-fine sandstone and minor conglomerate rock in the bottom (Figures 4(c) and 4(d)). The thickness of single-layer sandstone is relatively small, generally 1–8 m, with good sorting and roundness. Besides, it is rich in plant fossils and iron-bearing nodules, reflecting lacustrine sediment characteristics. The Taerga Formation is mainly gray-green, black-gray mudstone and gray-green siltstone and conformably contacted with the underlying Yangye Formation.

4.2. Mineral Composition and Organic Matter Features. The mineral composition of the six samples from Jurassic terrestrial shales in northern Kashi Sag is shown in Table 1. The results displayed that the clay mineral content is between 60 and 72%, with an average of 66%. The quartz content is between 25 and 35%, with an average of 29%. In general, the mineral composition of terrestrial shale is relatively stable, with clay minerals (chlorite + illite + kaolinite) as the main minerals, followed by brittle minerals (quartz + feldspar) (Table 1). Also, sample WQ-05 in the study contains a small amount of gypsum, suggesting that the climate was relatively dry at that time. The TOC of the Jurassic Kangsu Formation shale in Kashi Sag ranges from 1.42% to 3.36%, with an average value of 2.02%, which belongs to high-quality source rocks. The TOC of the Yangye Formation (4.27%) is higher than that of the Kangsu Formation in general. The R_o from the Kangsu and Yangye Formations were 0.849% and 0.788%, respectively, and both of them were in the mature stage (Table 1).

4.3. Reservoir Features. The results of isothermal adsorption tests are shown in Table 2 and Table 3. The total pore volume of the samples measured in this study ranges from 0.011 to 0.024 cm^3/g, with an average of 0.017 cm^3/g. According to the BJH (Barrett–Joyner–Halenda) model, the average pore size of terrestrial shale in the Wuqia area is between 9.10 and 12.83 nm, with an average of 11.10 nm (Table 2).

Compared with various calculation methods of specific surface area, the BET (Brunauer–Emmett–Teller) specific surface area can reflect it more accurately. Multipoint BET specific surface area = t – plot external area + t – plot total internal surface area of microporous. The specific surface area of the six samples BET specific surface area ranges from 5.46 to 14.31 m^2/g, with an average of 9.36 m^2/g. BJH unique circumference is more suitable for the analysis of pore size distribution. The six samples' BJH specific surface area ranges from 4.70 to 11.27 m^2/g, with an average of 7.27 m^2/g (Table 3).

Table 1: Minerals and geochemical characteristics of Jurassic shale in Kashi Sag.

Samples	Strata	TOC (%)	R_o (%)	Relative mineral content (%)					
				Chlorite	Illite	Kaolinite	Quartz	Feldspar	Gypsum
WQ-01	J_{1k}	1.42	$\frac{0.764-1.009}{0.897(16)}$	N.A.	N.A.	N.A.	N.A.	N.A.	N.A.
WQ-02	J_{1k}	1.61	$\frac{0.674-0.900}{0.785(13)}$	N.A.	N.A.	N.A.	N.A.	N.A.	N.A.
WQ-03	J_{1k}	1.67	$\frac{0.687-0.790}{0.728(4)}$	N.A.	N.A.	N.A.	N.A.	N.A.	N.A.
WQ-04	J_{1k}	3.36	$\frac{0.603-0.858}{0.742(11)}$	26	28	6	35	5	N.D.
WQ-05	J_{2y}	4.80	$\frac{0.678-0.851}{0.792(7)}$	25	34	6	26	4	5
WQ-06	J_{2y}	3.74	$\frac{0.882-0.928}{0.905(2)}$	24	38	10	25	3	N.D.

N.A.: not available; N.D.: not detectable.

Table 2: BJH pore volume of Jurassic shale in northern Kashi Sag.

Samples	Total volume (cm^3/g)	Microporous (cm^3/g)	Mesoporous (cm^3/g)	Macroporous (cm^3/g)	Average pore size (nm)
WQ-01	0.011	0.00120	0.006	0.0046	9.67
WQ-02	0.024	0.00025	0.016	0.0072	11.52
WQ-03	0.015	0.00015	0.009	0.0054	12.83
WQ-04	0.017	0.00014	0.012	0.0047	12.19
WQ-05	0.015	0.00010	0.012	0.0035	11.31
WQ-06	0.023	0.00026	0.017	0.0055	9.10

Table 3: Specific surface area of Jurassic shale in Kashi Sag (m^2/g).

Samples	BET specific surface area	*t*-plot specific surface area		BJH specific surface area			
		Microporous surface area	Surface area except microporous	Total specific surface area	Microporous	Mesoporous	Macroporous
WQ-01	5.46	4.59	0.87	4.70	3.47	1.05	0.18
WQ-02	13.91	4.32	9.58	10.69	2.34	8.06	0.28
WQ-03	7.94	2.37	5.57	5.39	1.16	4.02	0.21
WQ-04	8.17	2.20	5.97	6.14	0.99	4.97	0.18
WQ-05	6.34	0.95	5.39	5.43	0.77	4.55	0.12
WQ-06	14.32	3.38	10.94	11.27	1.78	9.28	0.20

5. Discussion

5.1. Characteristics of Jurassic Shale. Based on the lithologic character from two sections in this study, it was suggested that the strata of Jurassic in Kashi Sag were mainly continental sediments, and the organic-rich shale primarily developed in the Lower Jurassic Kangsu Formation and Middle Jurassic Yangye Formation, which is considered one of the three sets of the potential source rocks in Kashi Sag [27]. Comprehensive research shows that organic-rich shale in the Middle and Lower Jurassic continental facies is closely related to the paleo-sedimentary environment. Zhong et al. [40] considered the evolution of paleoclimate from dry (J_{1s}) to wet (J_{1k}–J_{2y}), and then to dry (J_{3kz}) in the Jurassic of the study area according to the color, lithology, sedimentary structure, paleontology, and geochemistry of rocks. The Early Jurassic Shalitashi Formation was attributed to the alluvial fan deposition under dry and oxidative conditions, which is not conducive to the deposition of organic-rich shale. During the Kangsu Formation deposition, it evolved into fluvial sediments, recording a humid climate and depositing dark shale with high organic matter content. Later, the basin showed difference between the north and the south in the Middle Jurassic. The northern basin was dominated by a freshwater environment, while a brackish–saline water environment dominated the southern basin. The paleoclimate evolved into

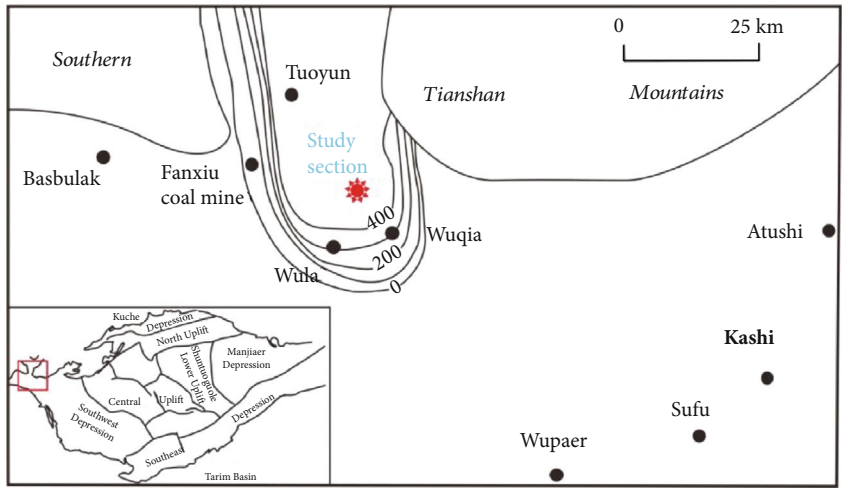

Figure 5: Thickness distribution of Middle and Lower Jurassic carbonaceous shale in northern Kashi Sag.

semihumid–semidry conditions, and the sedimentary facies changed from delta front to deep–semideep lacustrine and then to shore-shallow lake lacustrine. Therefore, the sedimentary shale of the Yangye Formation was characterized by the immense thickness and high content of organic matter. In the Late Jurassic, the basin evolved into fluvial and alluvial fan deposits in a dry and semidry environment, without shale sediments rich in organic matter. The whole sequence of Jurassic reflected a complete sedimentary cycle of shallow lacustrine–deep lacustrine–shallow lacustrine facies. The sedimentological observation in this study also confirms the above conclusion.

The water depth of the Yangye Formation in the Wuqia section is more significant than that of the Kangsu Formation, and the TOC content of the former is higher than that of the latter. Combined with previous research results, this study holds that the organic-rich strata are generally distributed in NW–SE direction, with multiple sedimentary centers (e.g., Yangye–Kuzigongsu and Yigeziya and Kekeya area). The high-quality source rocks have an excellent corresponding relationship with the semideep lacustrine and deep lacustrine environment, which are mainly developed in the piedmont fault basin system [29], along with the Talas–Fergana strike-slip fault system [31, 32]. The lacustrine carbonaceous shale is exposed in the Kuzigongsu graben zone, Keziletao graben zone, and the piedmont of the South Tianshan Mountains in the western part of Kangsu Town. The thickness of carbonaceous shale reached a maximum of more than 400 m in Wuqia Coal Mine of the northern Wuqia County, i.e., Kuzigongsu Graben. It decreases radially around and gradually pinches out at the Graben basin (Figure 5). Generally speaking, the northern part of Wuqia County is a favorable exploration area for shale gas because of its wide distribution and ideal shale thickness.

5.2. Features of the Organic Matter. TOC is one of the main indices for evaluating shale [43–45]. The content of TOC in Jurassic shale in the study area is high, which provides abundant substances for shale gas generation. According to Li and Zhang [4], the TOC of Lower Jurassic shale in Kashi Sag is generally more than 1.0%, the highest is greater than 5.0%, the chloroform asphalt "A" is between 0.001% and 0.1%, and the maximum hydrocarbon generation potential can reach 2.5 mg/g. The TOC of Middle Jurassic shale is mostly between 1.0% and 2.0%, and the hydrocarbon generation potential is above 0.5 mg/g. However, TOC in Kuzigongsu section is between 1.5% and 3.5%, with an average of 2.5%. Besides, according to the study of Xiao et al. [29], the average total organic carbon content of Jurassic shale in the Southwest Tarim Depression is 2.1%. These results are consistent with our conclusions. According to the criteria of Dong et al. [15], the lower limit of TOC content in shale gas production is 0.5%, and the better TOC content of gas-producing shale should be more than 2.0%. Therefore, according to the organic matter abundance standard, Jurassic shale in Kashi Sag belongs to high TOC shale. TOC content and organic-rich shale thickness control the self-sealing of shale [46]. The high TOC content and the great thickness also lead to the enhancement of the self-sealing ability of Jurassic shale. It is worth noting that the TOC of Jurassic shale in northern Kashi Depression is generally medium-good, but judging from the hydrocarbon generation potential ($S_1 + S_2$), extracted soluble organic matter (chloroform asphalt "A"), and total hydrocarbon (HC), the evaluation level of shale is lower than TOC, which may be affected by maturity. Generally speaking, for the early mature source rocks, the TOC evaluation results are not much different from those based on $S_1 + S_2$, chloroform asphalt "A," and HC. However, for mature–overmature samples, the evaluation result based on the latter will be lower than those found on the former, and the difference is more significant in the stage of high maturity or overmaturity [47, 48].

For the thermogenic shale gas system, organic matter's maturity is an important indicator to evaluate shale gas potential. A higher degree of thermal evolution is necessary for shale gas generation and organic pore formation [19]. Recent studies have investigated the types of Jurassic kerogen and thermal maturity of organic matter in northern Kashi Sag. The $\delta^{13}C_{org}$ of kerogen from the Kangsu Formation ranges from −20.7‰ to −25.5‰, with a mean of −23.3‰,

indicating that the organic matter in the Kangsu Formation may be kerogen type III. The Yangye Formation ranges from −25.5‰ to −28.1‰, with a mean of −25.8‰, indicating that the organic matter in the Yangye Formation is mainly kerogen type II_2 [22]. According to the microscopic observation of kerogen from Jurassic source rocks, Chen [49] claimed that the Lower Jurassic is mainly composed of vitrinite and inertinite, relatively low content of sapropelic and crustaceous materials, and is characterized by type III organic matter. The Middle Jurassic is mainly composed of vitrinite, and the content of inertinite is relatively low, showing the characteristics of type II-III organic matter. This phenomenon indicates that the source of organic matter has changed obviously with the deepening of lake water depth. Besides, the previous work suggested that the vitrinite reflectance values of the Kangsu Formation from the Kuzhigongsu section range from 1.3% to 1.8%, while the Yangye Formation ranges from 0.9% to 1.8% [4]. According to the samples collected by Da et al. [27], the average R_o of Jurassic in the Kuzigongsu section is 0.94%. These results are consistent with our test results (Table 1), indicating that the black shales in the sections are mature to highly mature (0.6%–1.0%, $n = 6$). Moreover, the mudstone in the sedimentary center has a high maturity, even reaching the stage of high maturity–overmaturity [50]. Thus, the thickness, kerogen type, TOC, and maturity of the black shales of the Kangsu and Yangye Formations in northern Kashi Sag indicate that these rocks are potential targets for exploration of shale gas.

5.3. Reservoir Brittleness. The intergranular pores of clay minerals in shale are well developed, but the cementation is complex, and the sorting is poor. Moreover, the clay minerals have a small particle size, strong plasticity, and water sensitivity, making the reservoir permeability decrease [51, 52]. In the late diagenetic stage, if there is no strong deformation, it is difficult for a single intergranular pore of clay minerals to have a good hydrocarbon migration ability. The specific surface area of clay minerals is larger than that of quartz minerals, and the more developed the intergranular pores, the stronger the gas adsorption capacity. The higher content of clay minerals is beneficial to developing the original microporous and microfractures in shale reservoirs (Figures 6(a) and 6(b)), which provide storage space for shale gas [43, 53, 54]. However, such a problem negatively impacts shale gas exploitation because it is not conducive to hydraulic fracturing, which is contrary to the implications of brittle minerals. Brittle minerals such as quartz and carbonate are prone to fracture under stress (Figure 6(c)).

On the one hand, the higher content of brittle minerals is beneficial to the development of microfractures and the improvement of reservoir performance; on the other hand, it is also helpful to the later exploitation of shale gas and achieves better fracture-making effect in the process of artificial fracturing [55, 56]. Compared with North American marine Barnett shale, the content of brittle minerals from Jurassic shale samples in the north of Kashi Depression is relatively low, which may be due to the deposition in a deep lake-semideep lake environment, far away from terrigenous denudation area. This situation reduces the input of many clastic materials, resulting in relatively high clay mineral content in the study's terrigenous shale.

The following formula in this study is selected to evaluate the brittleness index of the shale reservoir: Brittleness index $= (\text{quartz} + \text{feldspar} + \text{calcite} + \text{dolomite})/(\text{quartz} + \text{feldspar} + \text{calcite} + \text{dolomite} + \text{clay minerals}) \times 100\%$ [54, 57–60]. Through calculation, the shale's brittleness index of samples in the northern Kashi Sag ranges from 28.0% to 44.9%, with an average of 38.6% (Table 4). On the whole, it shows poor brittleness, which is not conducive to fracturing theoretically. Generally speaking, the evaluation of marine shale gas reservoir requires that the brittleness index in shale should be no less than 40% [57, 61, 62]. However, the evaluation method of marine shale gas cannot be simply copied in evaluating continental shale gas reservoirs. For example, Song et al. [63] found that the clay mineral content of continental shale is higher in general. Still, the brittle mineral content is lower, making the fracturing ability of shale worse than that of marine shale [53]. Therefore, the evaluation criteria of continental shale gas need to be further studied.

5.4. Characteristics of the Reservoir

5.4.1. Scanning Electron Microscope Observation. Through SEM observation of six samples of Jurassic shale in Tarim Basin, four types of reservoir space have been identified, i.e., organic pores, intergranular pores, intragranular pores, and microfractures. Organic pores are widely developed in organic-rich shale and are essential parts of shale reservoir space [64]. As shale gas can be adsorbed on the surfaces of mineral particle and organic matter, the porosity of organic matter directly controls adsorbed natural gas content [51, 65, 66].

In the study, the organic matter pores in the northern Kashi Sag are mostly nanoscale and round to oval. There are other irregular shapes, such as crescent shapes and slit shapes (Figures 7(a) and 7(b)). However, not all organic compounds have nanopores related to the maturity of organic compounds. For example, organic matter with low maturity usually contains fewer pores. Organic matter is mainly distributed on microbedding planes or microsedimentary discontinuity, and it is easy to form an interconnected pore network with strong permeability. The lipophilicity of organic matter makes organic matter's nanopore become the virtual storage space for natural gas [67, 68]. As the most important mineral component in Jurassic shale in this study, its highest content can reach 70.1%, and illite is the highest. Illite is usually flaky or fibrous, and slit or wedge-shaped pores are formed between the chips. In transforming montmorillonite into illite, the volume of minerals decreases, which leads to the formation of gaps between mineral particles (Figure 7(c)).

Intergranular pores are very abundant in young or shallow sediments, and they are usually well connected [69]. The irregular shape of intergranular pores and the large pore diameter of shale samples are beneficial to shale gas enrichment. In the process of diagenesis, the primary mineral crystals are subjected to physical and chemical actions such as mechanical collision, extrusion, and dissolution in acid or

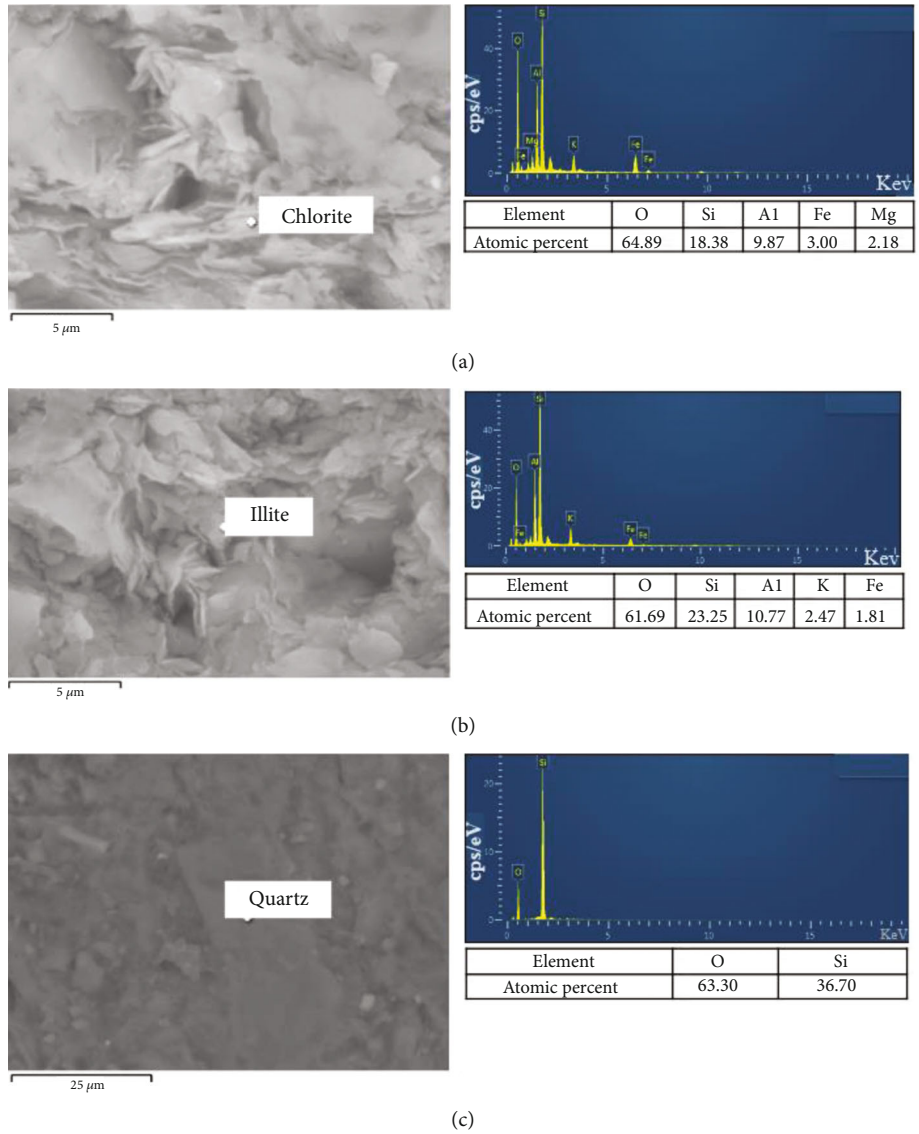

Figure 6: SEM images showing the mineralogical composition of the Jurassic shales in Wuqia section. (a) Bladed-shaped chlorite in the Kangsu Formation. (b) Filamentous illite in the Yangye Formation. (c) Quartz in the Kangsu Formation.

Table 4: Brittleness index of Jurassic shale in northern Kashi Sag (%) (S samples were collected by [29]).

Number	Mineral			Brittleness index
	Clay mineral	Quartz	Feldspar	
WQ-03	60	35	5	40.0
WQ-04	65	26	4	31.6
WQ-05	72	25	3	28.0
S-2 (J_{2y})	57.7	41.9	0.4	42.3
S-3 (J_{2y})	62.4	34.4	3.2	37.6
S-12 (J_{1k})	51.9	32.4	9.9	44.9
S-14 (J_{1k})	55.1	42.0	2.9	44.9
Mean	60.6	30.8	2.6	38.6

alkaline solution. And the crystals are broken or dissolved, forming a large number of intergranular pores. Intragranular pores mainly appear in irregular shapes and sizes of particles, mineral aggregates, and crystals (Figure 7(d)) [70]. The genetic types can be classified into primary and secondary. However, immediately after diagenesis, the number of pores in the particles was mostly destroyed and decreased, while the number of pores in the secondary particles increased. Because clay minerals are mainly distributed in cluster aggregates, many pores are distributed among internal clay crystal plates or plates. The morphology of these pores is primarily controlled by the crystal alignment [71].

In addition, fractures in shale samples are well developed and divided into structural fractures and diagenetic fractures. The former is mainly a wide range of macrocracks (Figure 7(e)). The latter is a fracture caused by the shrinkage of minerals. In the diagenetic process, the cause of formation is mainly caused by dry shrinkage, phase change, or

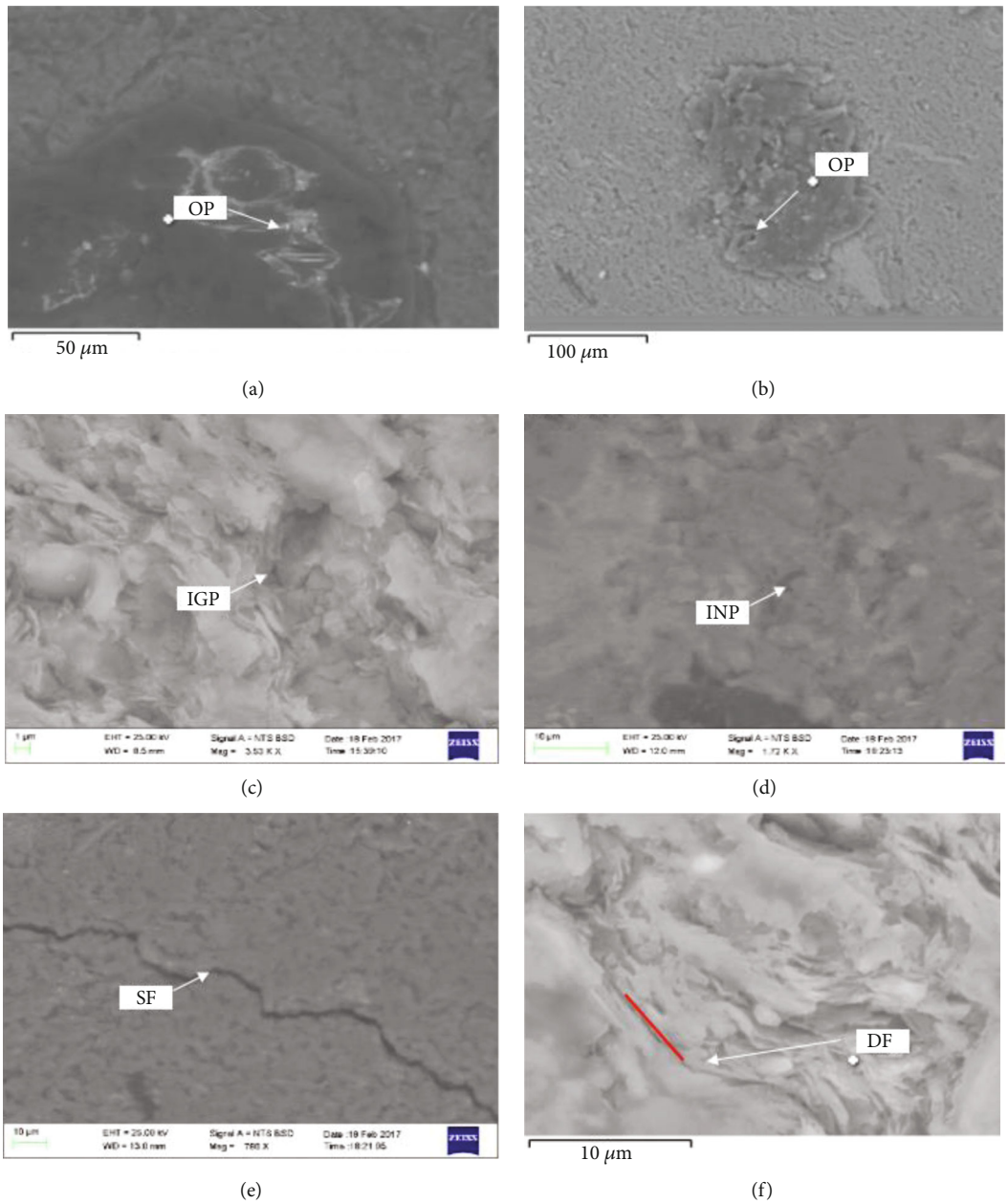

Figure 7: SEM images showing the pore types of Jurassic shales in Wuqia section. (a) Pore of organic matter (J_2y). (b) Pore of organic matter (J_1k). (c) Intergranular pore of illite-smectite mixed-layer mineral (I/S) (J_1k). (d) Intragranular pores of chlorite grain (J_1k). (e) Structural fracture (J_2y). (f) Diagenetic fracture (J_1k).

dehydrated minerals' thermal shrinkage (Figure 7(f)). The dehydration of clay minerals makes the volume smaller, which leads to more shrinkage microcracks with a width from 0.5 to 2 μm. Therefore, fracture plays a vital role in oil and gas production in shale reservoirs [72].

5.4.2. Pore Structure

(1) Adsorption Isotherm. According to the isothermal nitrogen adsorption-desorption curves of six samples (Figure 8), the pore type of samples can be analyzed [73–75]. All adsorption curves show inverted S-type, although they are slightly different in morphology. Based on a classification scheme [76], adsorption isotherm is divided into five types. In this study, the adsorption curve of shale samples in northern Kashi Sag is close to type II. In the low-pressure stage ($P/P_0 < 0.1$), the adsorption curve presents an upward convex shape, and nitrogen molecules are adsorbed by a monolayer. At this time, the adsorption amount is small. When the relative pressure $P/P_0 = 0.10 - 0.45$, nitrogen molecules begin to undergo multilayer adsorption, and the adsorption increment is small. When P/P_0 is in the range of 0.45–0.80, the adsorption curve is slightly concave and rises slowly. Multilayer adsorption of nitrogen

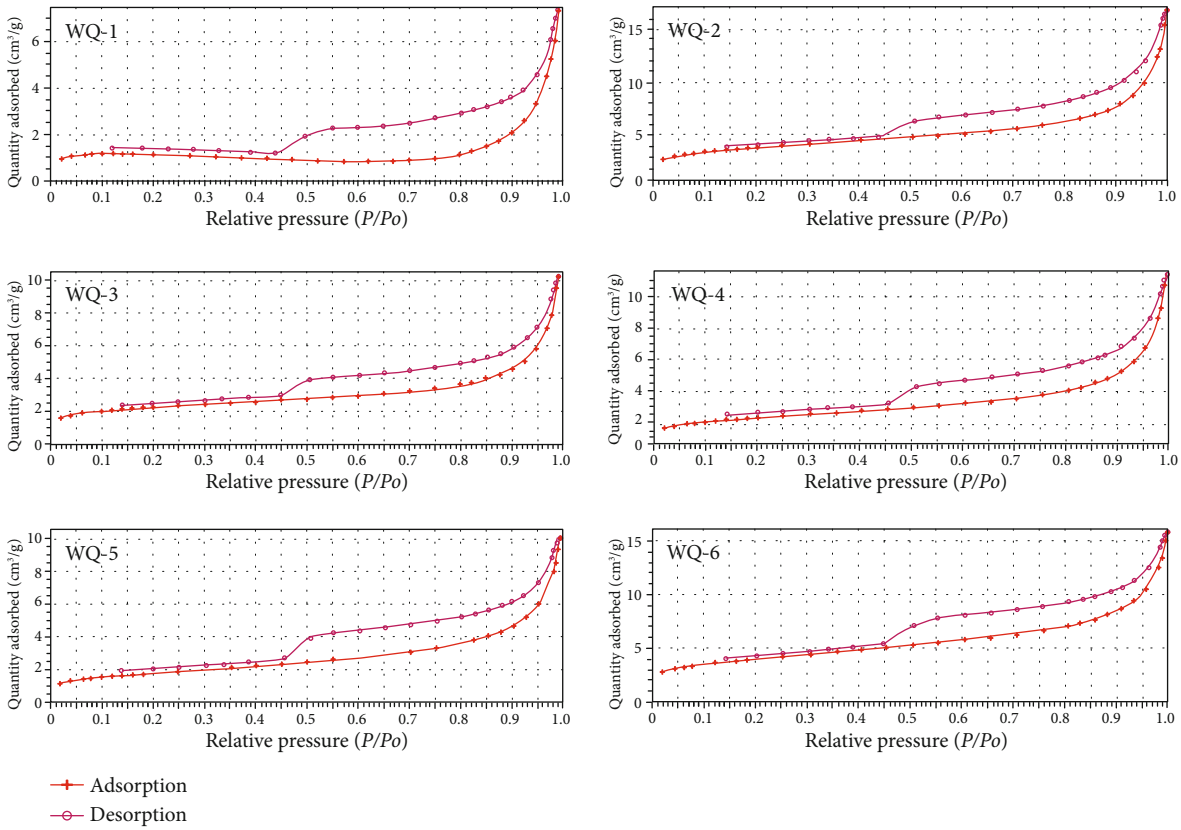

Figure 8: Nitrogen isothermal adsorption-desorption curves of Jurassic shale in Wuqia section.

molecules occurs, and the adsorption increment increases. When P/P_0 is in the range of 0.8–1.0, the adsorption curve rises rapidly, and the angle is concave. The nitrogen molecules are capillary condensed, and the adsorption capacity increases quickly. When P/P_0 reaches 0.9, the slope of the curve increases, and the adsorption capacity increases linearly [77]. The samples' adsorption curve and desorption curve do not coincide in high pressure, forming an adsorption loop (Figure 8).

The sorption isotherms have been classified by the International Union of Pure and Applied Chemistry (IUPAC) into six types, and the desorption isotherms into four categories designated H1 to H4 [78]. Different adsorption loop shape types reflect specific pore structure characteristics and type styles. The H1-type loop is often obtained from pore structures with regular size and arrangement. The H2-type loop is generally considered to be caused by porous adsorbate or homogeneous particle piled pores. Compared with H4-type, H3-type has a larger adsorption capacity at the high pressure, which is considered slit pores formed by stacking flaky particles. H4-type is also slit pores, which differ from the particle piled pore and are similar to those generated by layered structures. However, it is nearly impossible to describe the exact pore characteristics by a specific adsorption loop because of the complex pore morphology. In general, the adsorption curves of the six samples are very steep near the saturated vapor pressure, and the desorption curves are very steep at the medium pressure, which is close to the H3-type loop recommended by IUPAC and also has the characteristics of H4-type loop (between H3 and H4). Therefore, this form may be related to the superposition of the multiple standards loop, which is the comprehensive reflection of pore morphology. The above research shows that the pores of Jurassic shale gas reservoirs in Kashi Sag are mainly composed of nanopores characterized by irregular (amorphous) pores in structure; besides, the particle interior also has the characteristics of slit-like pores with parallel walls and contains other pores with various forms. Thus, this study suggested that this slit pore may be related to high clay mineral content in shale. Generally speaking, closed pores, including cylindrical pores with one end closed, parallel plate pores, and conical pores, cannot generate adsorption loops. However, all the six samples in this study displayed adsorption loops, which indicates that Jurassic continental shale gas reservoir's pore morphology was in an open state [79]. Those pores were mainly cylindrical pores with two ends empty and parallel plate pores with four sides hollow (i.e., cone, cylinder, plate, and ink bottle). Overall, this situation is conducive to improving the desorption efficiency of shale gas and the permeability of reservoirs, thus increasing production.

(2) Specific Surface Area and Pore Volume. The computing methods of the specific surface area mainly include multipoint BET, *t*-plot external surface area, the *t*-plot total

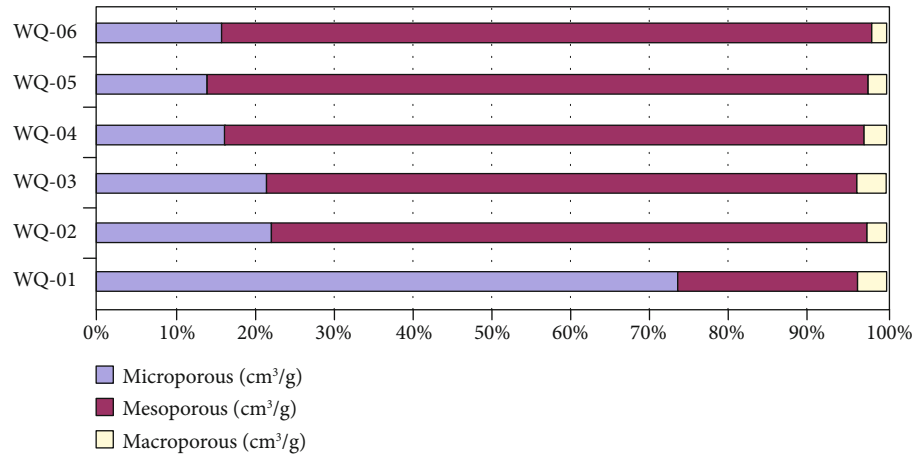

Figure 9: Specific surface area percentage of BJH pore in northern Kashi Sag.

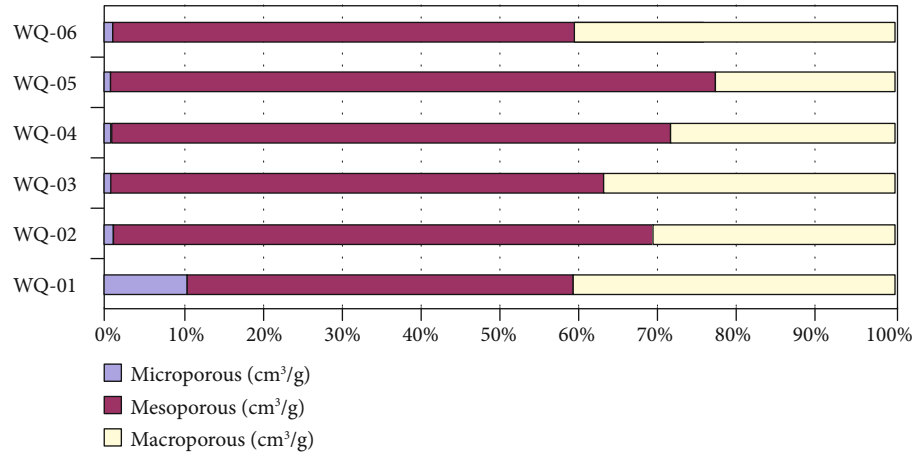

Figure 10: Volume percentage of BJH pore in northern Kashi Sag.

internal surface area of microporous, and BJH adsorption model. The multipoint BET method is the macroscopic total specific surface area, and BJH specific surface area is the total specific surface area of pores in a particular range. Generally, the BET method calculates the total specific surface area, and BET specific surface area = t − plot external area + t − plot total internal surface area of microporous. In contrast, the pore volume and pore size distribution are calculated by the BJH method. Therefore, compared with various calculation methods of specific surface area, BET specific surface area can reflect it more accurately and honestly [80–82]. According to the standards of the IUPAC, this study divides pores into microporous (<2.0 nm), mesoporous (2.0–50.0 nm), and macroporous (>50.0 nm) [78, 83]. After classifying the experimental data of Table 3, the pore-specific surface area percentages of macroporous, mesoporous, and microporous of each sample were calculated, respectively (Figure 9). As is shown in Table 3, the BET specific surface area of shale samples ranges from 5.46 to 14.31 m^2/g, with an average of 9.36 m^2/g. The adsorption capacity of shale is positively correlated with its specific surface area [84]. Therefore, the relatively high specific surface area of shale samples in Kashi Sag can improve the adsorption capacity of shale for methane. Meanwhile, according to the statistics of the specific surface area distribution of BJH, it can be seen that the mesopore's specific surface area occupies the majority. However, the specific surface area of microporous from the WQ-01 representative has a large percentage. After all, the minimum interval measured is 1.0 nm. In comparison, the minimum aperture of other samples measured is 1.7 nm. Therefore, the smaller pore-specific surface area of different samples was not measured. This also reflects that the actual proportion of microporous specific surface area is considerable. On the whole, microporous and mesoporous provide the central pore-specific surface area in this study.

The pore volume ratio of each pore size range is calculated separately, as shown in Figure 10. It can be seen that the mesoporous and macroporous provide the main pore volume in the Wuqia area. Concretely, the pore volume of microporous is relatively small, accounting for about 1%–10%. Thus, this study suggests that there may be two reasons to explain the small proportion of microporous. One is that the minimum pore size measured by the BJH method is

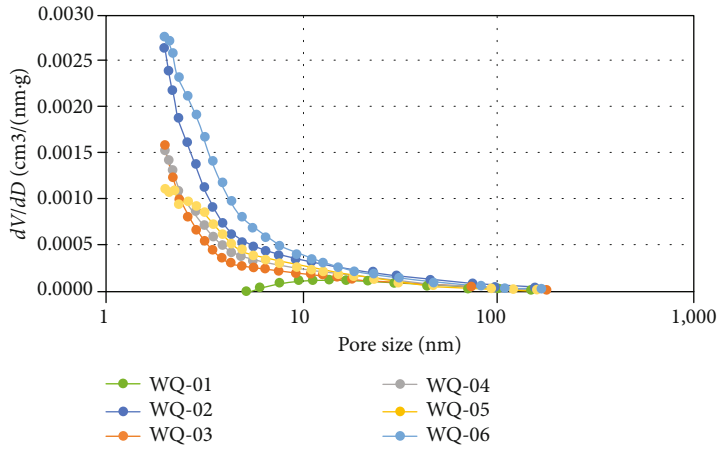

Figure 11: Frequency curve of BJH pore size distribution of shale samples in northern Kashi Sag.

1.7 nm (WQ-01 is 1.0 nm), and smaller pores are difficult to measure; on the other hand, according to the SEM observation, the distribution range of microporous is so tiny that its existence is rarely observed.

(3) Pore Size Distribution. The percentage of pore-specific surface area and volume in each pore size range cannot reflect all pore distribution frequencies. Therefore, the pore size distribution needs further analysis. The ordinate "dV/dD" in Figure 11 means the relative number of pores without considering the pore volume. On the whole, with the increase of pore diameter, the relative number of pores gradually decreases, indicating that the number of pores is mainly provided by the range of small pore diameter (2–8 nm). Therefore, the pore volume and specific surface area of mesoporous are primarily provided by small pore size. In contrast, the larger pore (8–50 nm) contributes less to the pore volume and specific surface area. When the pore diameter is close to 2 nm, the change rate of the pore volume of samples WQ-2–5 reaches the peak. This is because the minimum pore diameter of those samples is 1.98 nm. It can be speculated that when the pore diameter is less than 2 nm, the peak value will become larger; that is, the number of pores less than 2 nm is considerable. It is worth noting that since the minimum pore diameter of the WQ-01 sample is 6.61 nm, there may be deviation in the value of the WQ-01 sample.

6. Conclusions

In the northern Kashi Sag, the Middle and Lower Jurassic shale is a typical continental shale, mainly deposited in lake, river, and delta environments. The organic-rich shale primarily develops in the top of the Lower Jurassic and the lower part of the Middle Jurassic. This shale is generally more than 100 m and up to 400 m in thickness. The average total organic matter content is greater than 2%, R_o ranges from 0.6% to 1.8%, and organic matter is primarily II and III in kerogen types. Thus, the Middle and Lower Jurassic shale in the study has a good material basis for hydrocarbon generation. Meanwhile, the continental shale has a relatively high concentration of clay minerals, and the pores and fractures are well developed, which is conducive to the adsorption of shale gas. Microporous and mesoporous provide most of the specific surface area of shale, while mesoporous and macroporous provide most of the pore volume. The results referring to brittleness index, average pore volume, and specific surface area indicate that the reservoir's physical properties are relatively good. Overall, we propose that the Jurassic terrestrial shale in northern Kashi Sag has good-excellent shale gas exploration potential and development prospects.

Data Availability

All data, models, and code generated or used during the study appear in the submitted article.

Conflicts of Interest

The authors declare that they have no conflicts of interest.

Acknowledgments

This study was jointly supported by the Fundamental Research Funds for the Central Universities (No. 2021CDJQY-028) and the project "Research on the Investigation and Evaluation of Xinjiang Unconventional Energy Mineral Resources." We would like to thank the Xinjiang Bureau of Geo-exploration and Mineral Development for their help on the field.

References

[1] Z. J. Jin, Z. R. Bai, B. Gao, and M. W. Li, "Has China ushered in the shale oil and gas revolution?," *Oil& Gas Geology*, vol. 40, no. 3, pp. 451–458, 2019.

[2] C. N. Zou, R. K. Zhu, Z. Q. Chen et al., "Organic-matter-rich shales of China," *Earth-Science Reviews*, vol. 189, pp. 51–78, 2019, (in Chinese with English abstract).

[3] W. Z. Zhao, A. L. Jia, Y. S. Wei, J. L. Wang, and H. Q. Zhu, "Progress in shale gas exploration in China and prospects for future development," *China Petroleum Exploration*, vol. 25, no. 1, pp. 31–43, 2020.

[4] H. X. Li and Y. W. Zhang, "Global shale gas exploration and development today and China's shale gas development strategy," *Sino-Global Energy*, vol. 5, pp. 22–29, 2015.

[5] C. Z. Yan, Y. Z. Huang, C. M. Ge, D. Z. Dong, and K. M. Cheng, "Shale gas: enormous potential of unconventional natural gas resources," *Natural Gas Industry*, vol. 29, no. 5, pp. 1–7, 2009.

[6] H. K. Nie, Z. L. He, G. X. Liu et al., "Status and direction of shale gas exploration and development in China," *Journal of China University of Mining & Technology*, vol. 49, no. 1, pp. 14–35, 2019.

[7] X. Wu, Z. Y. Ren, and Y. Wang, "Situation of world shale gas exploration and development," *Resource & Industries*, vol. 15, no. 5, pp. 61–67, 2013.

[8] L. Zhang, J. Li, Z. Li, J. Zhang, R. Zhu, and Y. Bao, "Advances in shale oil/gas research in North America and considerations on exploration for continental shale oil/gas in China," *Advance in Earth Science*, vol. 6, pp. 700–711, 2014.

[9] X. X. An, W. H. Huang, S. Y. Liu, and H. Y. Jiang, "The distribution, development and expectation of shale gas resources," *Resources & Industries*, vol. 12, no. 2, pp. 103–109, 2010.

[10] D. X. Zhang and T. Y. Yang, "An overview of shale-gas production," *Acta Petrolei Sinica*, vol. 34, no. 4, pp. 792–801, 2013.

[11] Y. Song, Z. Li, Z. X. Jiang, Q. Luo, D. D. Liu, and Z. Y. Gao, "Progress and development trend of unconventional oil and gas geological research," *Petroleum Exploration and Development*, vol. 44, no. 4, pp. 638–648, 2017.

[12] Z. F. Wei, Y. L. Wang, G. Wang et al., "Enrichment mechanism of the Upper Carboniferous-Lower Permian transitional shale in the east margin of the Ordos Basin, China: evidence from geochemical proxies," *Geofluids*, vol. 2020, article 8867140, 14 pages, 2020.

[13] D. Z. Dong, C. N. Zou, Y. Yang et al., "Progress and prospects of shale gas exploration and development in China," *Acta Petrolei Sincia*, vol. S1, pp. 107–114, 2012.

[14] D. Zhao, Y. Guo, Y. Zhu, G. Wang, X. Chong, and X. Hu, "Analysis of micro-scale heterogeneity characteristics in marine shale gas reservoir: pore heterogeneity and its quantitative characterization," *Journalof China University of Mining & Technology*, vol. 47, no. 2, pp. 296–307, 2018.

[15] D. Dong, Y. Wang, X. Huang et al., "Discussion about geological characteristics, resource evaluation methods and its key parameters of shale gas in China," *Natural Gas Geoscience*, vol. 9, pp. 1583–1601, 2016.

[16] W. X. Hu, S. P. Yao, X. C. Lu, H. G. Wu, F. N. Sun, and J. Jin, "Effects of organic matter evolution on oil reservoir property during diagenesis of typical continentalshale sequences," *Oil & Gas Geology*, vol. 40, no. 5, pp. 947–956, 2019.

[17] Q. Zhang, F. Wang, Z. Xiao, Y. Lu, and Y. Wu, "The discussion of natural gas source in Well Ake 1," *Natural Gas Geoscience*, vol. 6, pp. 484–487, 2003.

[18] J. F. Zhang, D. L. Wang, Z. M. Wang, X. Li, and X. F. Su, "Natural gas deposit formation geochemistry of Akmomu gas field Kashi Sag in Tarim Basin," *Natural Gas Geoscience*, vol. 4, pp. 507–513, 2005.

[19] W. Liu, F. Yang, J. C. Wu, and H. Z. Xiao, "The discussion on natural gas source in Akmomu gasfield, northern margin of Kashi Sag," *Natural Gas Geoscience*, vol. 3, pp. 486–494, 2015.

[20] L. Qian, Y. H. Lu, L. C. Huang et al., "Source and gathering features of Kelatuo natural gas in the Kashi Sag, Tarim Basin," *Chinese Journal of Geology*, vol. 42, no. 2, pp. 253–266, 2007.

[21] J. H. Luo, Z. C. Che, and L. Liu, "The origin of Kashi Depression and the guide for exploration," *Northwest University (Natural Science Edition)*, vol. 5, pp. 69–72, 1998.

[22] M. M. Meng, Z. H. Kang, Y. H. Xu, C. Yu, and Q. Liu, "Geochemical characteristics of source rocks and oil-source correlation in the Kashi Sag, Tarim Basin," *Petroleum Geology and Experiment*, vol. 38, no. 2, pp. 266–273, 2016.

[23] M. H. Sun, *The Study on Sequence Stratigraphy and Sedimentary System of Mid-Lower Jurassic in Southwestern Tarim*, Xinjiang University, 2013.

[24] J. M. Zhan, X. Q. Li, and Q. Zhou, "The study on hydrocarbon generation history of Jurassic coal measures source rocks in Kashi Sag," *Journal of Anhui University of Science and Technology (Natural Science)*, vol. 2, pp. 1–4, 2005.

[25] C. Wu, S. M. Zhai, B. Qiu, Y. Hong, W. Xiao-yun, and L. Song, "Hydrocarbon evaluation of Kashi Sag in Tarim Basin," *Xinjiang Petroleum Geology*, vol. 24, no. 3, pp. 221–223, 2003.

[26] T. J. Li and X. R. Luo, "The Jurassic petroleum system in the Kashi Depression of the Tarim Basin," *Petroleum Geology and Experiment*, vol. 1, pp. 39–43, 2005.

[27] J. Da, Y. Song, M. J. Zhao, G. Y. Fu, and Z. L. Yang, "Evolution and potential discussion of hydrocarbon source rock in north margin of Kashi Sag, Tarim Basin," *Xinjiang Petroleum Geology*, vol. 1, pp. 77–80, 2007.

[28] X. Y. Gao, L. F. Liu, X. Q. Shang, Y. Wang, T. X. Su, and Q. W. Dai, "Characterization of Jurassic shale reservoirs and the geological background of shale gas accumulations in Tarim Basin," *Acta Petrolei Sinica*, vol. 4, pp. 647–659, 2013.

[29] W. Y. Xiao, X. X. Lv, Z. K. Bai, Y. F. Wang, and J. Tu, "Characteristics of Jurassic shales and potential of shale gas in Southwest Depression of Tarim Basin," *Journal of China Coal Society*, vol. 41, no. z2, pp. 491–501, 2016.

[30] X. Y. Zhou, J. H. Luo, and G. R. Mai, "Tectonic characteristics and petroleum geology of Kashi Sag and its surrounding areas in Tarim basin. Version 1," Petroleum Industry Press, Beijing, 2005.

[31] J. H. Luo, X. Y. Zhou, B. Qiu, Z. L. Yang, H. Yin, and X. L. Shang, "Structural features of fold-thrust zone in Kashi Depression, western Tarim Basin," *Oil & Gas Geology*, vol. 2, pp. 199–203, 2004.

[32] X. B. Li, "Petroleum geology characteristics of Kashi Depression," *Xinjiang Petroleum Geology*, vol. 4, pp. 285–289, 1995.

[33] X. A. Chen, X. L. Zhang, and Q. P. Qu, "Characteristics of Piedmont structure and hydrocarbon prospect in the southwest of the Tarim Basin," *Xinjiang Petroleum Geology*, vol. 20, no. 6, pp. 468–472, 1999.

[34] X. Y. Zhou, Y. Z. Hu, S. Liu et al., *Petroleum geology in the northern outcrop area of Kashi Sag, Tarim Basin. Version 1*, Petroleum Industry Press, Beijing, 2003.

[35] D. W. Lv, Y. Song, L. Q. Shi, Z. Wang, P. Cong, and A. J. T. van Loon, "The complex transgression and regression history of the northern margin of the Palaeogene Tarim Sea (NW China), and implications for potential hydrocarbon occurrences," *Marine and Petroleum Geology*, vol. 112, p. 104041, 2020.

[36] Y. Ding, J. P. Gong, and H. Wang, "Synthetic evaluation of source rocks in Southwest Depression of the Tarim Basin," *Petroleum Geology and Experiment*, vol. 4, pp. 336–339, 1999.

[37] D. Z. Dong and A. C. Xiao, *Petroleum Geology and Petroleum Resources in the Southwest Depression of Tarim Basin*, Petroleum Industry Press, Beijing, 1st edition, 1998.

[38] W. Z. Zhao and G. Y. Zhang, *Passive Continental Margin Evolution and Petroleum Geology: A Case Study of Southwestern Tarim Basin*, Petroleum Industry Press, Beijing, 1st Ed edition, 2007.

[39] T. S. Yong, "Carboniferous lithofacies palaeogeography and its oil-bearing properties of Tarim platform," *Xinjiang Petroleum Geology*, vol. 3, pp. 13–24, 1983.

[40] D. K. Zhong, X. M. Zhu, G. W. Wang, and Q. B. Xie, "Paleoenvironments of Jurassic of Kashi Sag in Tarim Basin," *Journal of Palaeogeography*, vol. 4, pp. 47–54, 2002.

[41] D. K. Zhong, X. M. Zhu, Z. G. Shen, J. S. Chen, and L. Zhou, "Sedimentation and evolution of the Jurassic in the Kashi Depression, Tarim Basin," *Chinese Journal of Geology (Scientia Geologica Sinica)*, vol. 3, pp. 385–391, 2003.

[42] B. S. Sun, Z. R. Liu, and Z. M. Wang, "New knowledge on geology of Kashi Depression in southwest Tarim," *Xinjiang Geology*, vol. 1, pp. 78–84, 2003.

[43] P. C. Hackley, "Geological and geochemical characterization of the Lower Cretaceous Pearsall Formation, Maverick Basin, South Texas: a future shale gas resource," *AAPG Bulletin*, vol. 19, no. 5, pp. 1428–1449, 2012.

[44] D. Strapoc, M. Mastalerz, and A. Schimmelmann, "Geochemical constraints on the origin and volume of gas in the New Albany Shale (Devonian–Mississippian), eastern Illinois Basin," *AAPG Bulletin*, vol. 94, no. 11, pp. 1713–1740, 2010.

[45] D. W. Lv, Z. X. Li, D. D. Wang et al., "Sedimentary model of coal and shale in the Paleogene Lijiaya Formation of the Huangxian Basin: insight from petrological and geochemical characteristics of coal and shale," *Energy & Fuels*, vol. 33, no. 11, pp. 10442–10456, 2019.

[46] K. Zhang, C. Jia, Y. Song et al., "Analysis of Lower Cambrian shale gas composition, source and accumulation pattern in different tectonic backgrounds: a case study of Weiyuan Block in the Upper Yangtze region and Xiuwu Basin in the Lower Yangtze region," *Fuel*, vol. 263, article 115978, 2020.

[47] W. Z. Zhao, C. N. Zou, and Y. Song, *Advances in Theories and Methods of Petroleum Geology*, Petroleum Industry Press, Beijing, 1996.

[48] D. M. Jarvie, "Shale resource systems for oil and gas: part 1—shale-gas resource systems," *AAPG Memoir*, vol. 97, pp. 69–87, 2012.

[49] C. Chen, *Comprehensive Evalution and Regionalization of Shale Gas Resources in Tarim Basin (Engineering Master Thesis)*, China University of Petroleum (EastChina), 2013.

[50] M. J. Zhao, Z. M. Wang, Y. Song et al., "Source and accumulation of oil and gas in Kashi Sag, Tarim Basin, NW China," *Petroleum Exploration and Development*, vol. 2, pp. 50–54, 2005.

[51] S. Chen, Y. Zhu, H. Wang, H. Liu, W. Wei, and J. Fang, "Shale gas reservoir characterisation: a typical case in the southern Sichuan Basin of China," *Energy*, vol. 36, no. 11, pp. 6609–6616, 2011.

[52] W. D. Zhang, M. Guo, and Z. X. Jiang, "Parameters and method for shale gas reservoir evaluation," *Natural Gas Geoscience*, vol. 22, no. 6, pp. 1093–1099, 2011.

[53] X. M. Xiao, Z. G. Song, Y. M. Zhu, and H. W. Yin, "Summary of shale gas research in North American and revelations to shale gas exploration of Lower Paleozoic strata in China south area," *Journal of China Coal Society*, vol. 5, pp. 721–727, 2013.

[54] S. Q. Wang, S. Y. Wang, and L. Man, "Appraisal method and key parameters for screening shale gas play," *Journal of Chengdu University of Technology (Science & Technology Edition)*, vol. 40, no. 6, pp. 609–620, 2013.

[55] S. L. Montgometry, D. M. Jarvie, K. A. Bowker, and R. M. Pollastro, "Mississippian Barnett Shale, Fort Worth Basin□North Central Texas: gas-shale play with multi–trillion cubic foot potential," *AAPG Bulletin*, vol. 2, no. 89, pp. 155–175, 2005.

[56] E. A. Letham and R. M. Bustin, "Klinkenberg gas slippage measurements as a means for shale pore structure characterization," *Geofluids*, vol. 16, no. 2, pp. 264–278, 2016.

[57] Y. Tu, H. Y. Zou, H. P. Meng, Z. Xia, and N. Li, "Evaluation criteria and classification of shale gas reservoirs," *Oil & Gas Geology*, vol. 1, pp. 153–158, 2014.

[58] R. Lewis, D. Ingraham, M. Pearcy, J. Williamson, W. Sawyer, and J. Frantz, "New evaluation techniques for gas shale reservoirs," in *Reservoir Symposium*, pp. 1–11, Schlumbcrgcr Houston, 2004.

[59] Y. X. Li, J. C. Zhang, S. L. Jiang, and S. B. Han, "Geologic evaluation and targets optimization of shale gas," *Earth Science Frontiers*, vol. 19, no. 5, pp. 332–338, 2012.

[60] M. D. Bunaman, W. Xia, and J. Shelton, "Shale gas play screening and evaluation criteria," *China Petroleum Exploration*, vol. 14, no. 3, pp. 51–64, 2009.

[61] D. J. Hou, S. J. Bao, X. P. Mao et al., "Discussion on the key issues of resource potential evaluation for shale gas," *Journal of Earth Sciences and Environment*, vol. 3, pp. 7–16, 2012.

[62] S. F. Lu, W. B. Huang, F. W. Chen et al., "Classification and evaluation criteria of shale oil and gas resources: discussion and application," *Petroleum Exploration and Development*, vol. 39, no. 2, pp. 249–256, 2012.

[63] Y. Song, F. L. Gao, X. L. Tang, L. Chen, and X. M. Wang, "Influencing factors of pore structure differences between marine and terrestrial shale reservoirs," *Acta Petrolei Sinica*, vol. 41, no. 2, pp. 1501–1512, 2020.

[64] R. Gareth, R. Chalmers, M. Bustin, and I. M. Power, "Characterization of gas shale pore systems by porosimetry, pycnometry, surface area, and field emission scanning electron microscopy/transmission electron microscopy image analyses: examples from the Barnett, Woodford, Haynesville, Marcellus, and Doig units," *AAPG Bulletin*, vol. 96, no. 6, pp. 1099–1119, 2012.

[65] H. K. Nie, Z. J. Jin, and J. C. Zhang, "Characteristics of three organic matter pore types in the Wufeng-Longmaxi shale of the Sichuan Basin, southwest China," *Scientific Reports*, vol. 8, no. 1, article 7014, 2018.

[66] X. P. Luo, P. Wu, J. H. Zhao, and N. Yang, "Study advances on organic pores in organic matter-rich mud shale," *Journal of Chengdu University of Technology (Science & Technology Edition)*, vol. 42, no. 1, pp. 50–59, 2015.

[67] H. Kumar, D. Elsworth, J. P. Mathews, and C. Marone, "Permeability evolution in sorbing media: analogies between organic-rich shale and coal," *Geofluids*, vol. 16, pp. 43–55, 2015.

[68] Y. J. Han, B. Horsfield, R. Wirth, N. Mahlstedt, and S. Bernard, "Oil retention and porosity evolution in organic-rich shales," *AAPG Bulletin*, vol. 101, no. 6, pp. 807–827, 2017.

[69] C. Luo, S. G. Liu, and Z. L. Luo, "Pore structure characteristics of black shale in the Lower Cambrian Niutitang Formation of Nangao section in Danzhai, Guizhou Province," *Geological Science and Technology Information*, vol. 33, no. 3, pp. 93–105, 2014.

[70] P. Luo and L. M. Ji, "Reservoir characteristics and potential evaluation of continental shale gas," *Natural Gas Geoscience*, vol. 24, no. 5, pp. 1060–1068, 2013.

[71] R. G. Loucks, R. M. Reed, S. C. Ruppel, and D. M. Jarvie, "Morphology, genesis, and distribution of nanometer-scale pores in siliceous mudstones of the Mississippian Barnett Shale," *Journal of Sedimentary Research*, vol. 79, no. 12, pp. 848–861, 2009.

[72] J. B. Curtis, "Fractured shale-gas systems," *AAPG Bulletin*, vol. 86, no. 11, pp. 1921–1938, 2002.

[73] D. Brown, "Research getting unconventional boost," *American Association of Petroleum Geologists Explorer*, vol. 31, p. 810, 2010.

[74] H. K. Nie, J. C. Zhang, X. B. Ma, and R. K. Bian, "A preliminary study of negative adsorption phenomena of shale adsorption gas content by isothermal adsorption," *Earth Science Frontiers*, vol. 6, pp. 282–288, 2013, (in Chinese with English abstract).

[75] Q. L. Zhang, "The analysis of abnormal phenomena in shale isothermal absorption volumetry test," *Coal Geology & Exploration*, vol. 43, no. 5, p. 3133, 2015.

[76] D. H. Brunauer, "The four seasons of Marina Forrester," *Journal of Evolutionary Psychology*, vol. 15, no. 1-2, pp. 54–59, 1994.

[77] L. Cao and Y. H. Guo, "Study on pore structure characteristics of mud shale in Wuxiang Block of eastern Qinshui Basin," *Coal Science and Technology*, vol. 48, no. 4, pp. 230–236, 2020.

[78] J. Rouquerol, D. Avnir, C. W. Fairbridge et al., "Physical chemistry division commission on colloid and surface chemistry, subcommittee on characterization of porous solids: recommendations for the characterization of porous solids," *International Union of Pure and Applied Chemistry*, vol. 68, pp. 1739–1758, 1994.

[79] S. B. Chen, Y. M. Zhu, H. Y. Wang, H. L. Liu, W. Wei, and J. H. Fang, "Structure characteristics and accumulation significance of nanoporesin Longmaxi shale gas reservoir in the southern Sichuan Basin," *Journal of China Coal Society*, vol. 37, no. 3, pp. 438–444, 2012.

[80] J. H. De Boer, D. H. Everett, and F. S. Stone, *The Structure and Properties of Porous Materials*, DH Everett, FS Stone, 1958.

[81] E. P. Barrett, L. G. Joyner, and P. P. Halenda, "The determination of pore volume and area distributions in porous substances: I. Computations from nitrogen isotherms," *Journal of the American Chemical Society*, vol. 73, pp. 373–380, 1951.

[82] W. J. Thomas and B. Crittenden, *Adsorption Technology and Design*, Elsevier Science & Technology, 1998.

[83] S. Lu, J. Li, P. Zhang et al., "Classification of microscopic porethroats and the grading evaluation on shale oil reservoirs," *Petroleum Exploration and Development*, vol. 45, no. 3, pp. 436–444, 2018.

[84] Y. L. Kang, Y. B. Chen, X. C. Li, L. J. You, and M. J. Chen, "Effect of particle size on methane sorption capacity of shales," *Natural Gas Geoscience*, vol. 28, no. 2, pp. 272–279, 2017.